Supporting Information

Ramanathan *et al.* 10.1073/pnas.0807193106

SI Text

Supplementary Discussion of the Diffusion Model. As a consequence of our experimental observations, we propose 1D diffusion as the dominating mechanism for intersite communication by Type III restriction enzymes and rule out significant contributions from active translocation. In this section we will sketch out our diffusion model in more detail, make testable predictions for future experiments and present additional experimental data in support of 1D diffusion.

A more detailed illustration of our model is shown in the supporting information (SI) Fig. S6 and contains the following main steps:

1. Each enzyme will associate with the DNA in an orientated fashion, determined by the binding sites, each with a concentration dependent rate k_{on}.
2. An enzyme switches into the diffusion mode (orange oval) with rate k_{ini}. We speculate that this is triggered by ATP binding and/or hydrolysis, which causes a conformational change of the enzyme. Such ATP hydrolysis state-dependent switching to diffusion has also been observed in DNA-mismatch repair (1) and for the kinesin related motor protein MCAK (2). Both these systems have a greatly reduced ATPase rate compared with expectations for equivalent linear motors. We therefore think that Type III restriction enzymes might have evolved similarly to use the slow ATPase activity of their motor domains to trigger diffusion.
3. Enzyme(s) diffuse along DNA in a 1D bidirectional random walk with a rate constant k_{slide}. During this sliding on uncapped DNA, the enzyme can reach the DNA end and dissociate with $k_{off,end}$. We anticipate that simple dissociation (k_{off}) during sliding occurs less frequently, because DNA end-capping has a considerable influence even over distances of several thousand bp. Because the enzyme does not let go of the DNA track during sliding, the original orientation defined by the recognition site is maintained. Diffusion can be a very fast process (see below), with distances of >1 kb covered within a few seconds (1).
4. Eventually, if dissociation has not occurred, the diffusing enzyme may encounter a second enzyme bound at a site distant from the initiation of sliding.
5. If this enzyme is bound in the correct orientation (HtH), cleavage will be triggered. At a minimum, ATP binding by the second enzyme should be required based on the observation that both enzymes have to be able to bind and potentially hydrolyze ATP (3).
6. Finally, the DNA is cut close to the site of the nondiffusing enzyme, each enzyme cutting one strand. The ATPase rate of the Type III REs may be limited by the absolute nucleotide hydrolysis rate, or by a slow rate of DNA binding. This model allows DNA cleavage to be triggered following the hydrolysis of only a few ATPs (e.g., with *Eco*PI). More ATP may be required (e.g., with *Eco*P15I) because of futile communication events (i.e., multiple sliding cycles are required before a successful interaction).

This model can readily explain our experimental observables: (i) Absence of DNA looping and force independence of DNA cleavage; (ii) Bidirectional communication between target site and DNA end; and (iii) Extremely low ATPase rates. Furthermore, in contrast to previous models, it can also explain all of the bulk solution data on Type III REs thus far. This includes the original Lac repressor roadblock experiments that were used to establish the dogma (4). Even more importantly, it can also explain the observation that two immediately adjacent Type III restriction enzyme sites and, over short distances, sites in a tail-to-tail configuration, can be cleaved (5). In the case of immediately adjacent sites (i.e., with an intersite spacing of 0 bp), when one enzyme associates with the target site it will block binding of the second enzyme at its oppositely oriented target site. However, upon initiation, diffusion of the first enzyme away from its site will clear the second site for the second enzyme that can then bind and wait for the eventually returning first enzyme. In this model, 50% of the first enzymes will diffuse in the "wrong" direction, resulting in unproductive collisions—indeed, the data in ref. 5 shows that the cleavage is only 50% as active as normal. In a similar manner, cleavage of tail-to-tail oriented pairs of sites can be explained. The first enzyme just needs to diffuse, on average, in the direction of its tail and past the second site, so that it can then collide with a later-associating enzyme at the second target site. Because the first enzyme never released the DNA, the collision is in the permissive head-to-head orientation despite having originated from a tail-to-tail pair of sites.

In the following we discuss a few details of the model, which might not be obvious at the first glance.

Time Required for Diffusive Intersite Communication. Is the velocity of diffusive intersite communication fast enough to ensure the rapid DNA cleavage which we observe in our experiments? Only recently with the development of single molecule technologies has it been possible to determine diffusion coefficients for a few enzymes such as hOGG1 (6), Rad51 (7), Msh2-Msh6 (1), p53 (8), UL42 (9), and *Eco*RV (10). With the exception of Rad51, which exhibited a relatively slowly diffusing population, the observed diffusion coefficients (D) were between $1{\cdot}10^5$ bp^2 s^{-1} and $5{\cdot}10^6$ bp^2 s^{-1}. The average time required to move away a certain distance (d) from the start site is called the first passage time and is given by (11, 12):

$$\tau = \frac{d^2}{2D}$$

This provides first passage times of between 0.1 and 6 s for a 1,100-bp distance. However, this is only the time to move 1,100 bp either leftward or rightward on the DNA. To calculate the time to find a target site on a specific side of the starting point, one has to consider that the diffusing enzyme will on average also spend "nonproductive" time sliding on the wrong side. For capped DNA ends in which we treat the cap as a reflecting wall, the first passage time becomes (11):

$$\tau_{end} = \frac{1}{2D}(d^2 + 2de)$$

where e is the location of the start site from the reflecting DNA end. Considering the above range of diffusion constants and the 5.7 kbp DNA substrate used here, where e is approximately 2,000 bp, provides a mean time of between 0.5 and 30 s to communicate between the two sites 1,100 bp apart. Given our mean cleavage times of 2–3 min, the actual diffusion process will most likely be faster than the total cleavage process. Thus, potentially,

diffusion can be a much faster communication mechanism than translocation for the length scales considered.

Cleavage Site Selection. How does the model explain the precise location of the cleavage site downstream of the target sequence? If the initiation process is relatively fast compared with the communication time, then both enzymes will be likely to initiate at similar times and so most collisions occur away from the target site. For example, Type I restriction enzymes produce such a random cleavage pattern originating from random collision positions (13). However, we note that the collision position very much depends on the initiation rate of the enzyme, which determines the time it stays bound at the target site, and the bidirectional random walk stepping rate determined by the diffusion coefficient ($k_{step} = 2D/bp^2$, for diffusion involving single bp steps). Indeed simulations show that at high ratios between k_{step} and k_{ini}, collisions will occur mainly at the target sites (Fig. S7). Given diffusion coefficients of up to $5{\cdot}10^6$ bp^2 s^{-1}, cleavage at the target site would already be achieved for initiation rates as fast as 10 s^{-1}. However, as the intersite distance is increased, the number of collisions away from the target sites would also increase. We therefore suggest that cleavage is not triggered upon collision between any two enzymes, but rather requires that one enzyme is still bound to its target site. We envision a rather dynamic situation in which enzymes bind to the target sites and start to diffuse, allowing even more enzymes to bind until eventually one of them collides with a target-site bound enzyme, resulting in cleavage only if the relative enzyme orientation is correct. While the original site binding orientation is retained, the exact origin of the enzyme is not. The probability of a collision event is therefore a function of lifetime on the DNA during sliding and lifetime on the recognition site before initiation. Conditions that increase these times (e.g., end capping) will favor DNA cleavage.

Cleavage Kinetics as a Function of Intersite Spacing and DNA End Length. So far, all support for the diffusion model has been indirect, by ruling out alternative communication mechanisms such as 3D looping and directional translocation. Although we think that, given the constraints set by our data so far, only diffusion remains possible as an intersite communication mechanism, a more direct support for diffusion would be desirable. For example, the influence of end capping could still be explained within the framework of a translocation model by allowing the enzyme to translocate to the end and to turn around or move backwards to the other target site (although this would still not explain the extremely low ATPase activity).

To distinguish directional translocation from diffusion motion, one could use the different dependencies of the communication time on the intersite spacing. For directional translocation, the communication time will increase in a simple linear fashion with distance. For example, this is seen for the DNA translocating Type I restriction enzymes in bulk translocation experiments (14) and in bulk cleavage experiments (F. Peske and MDS, unpublished observation) as a characteristic lag time which has a linear dependence on the spacing between start and target site. In the case of diffusive communication, such a lag should not be observable because the bidirectional motion underlying diffusion leads to desynchronization of the enzyme population. Furthermore, if the diffusive communication step is rate-limiting for the whole cleavage process, one would not expect a linear relationship but rather a quadratic dependence of the cleavage rate on the intersite distance according to *SI Text* Eqs. **1** and **2**. To test for the presence of distance-dependent lags and the dependence of the cleavage rate on the intersite distance, we carried out additional cleavage experiments on substrates with 1.1-kb and 3.3-kb intersite spacing (Fig. S8*a*). In the case of capped DNA substrates, *SI Text* Eq. **2** predicts that the more distant sites should be cleaved at a >3-fold slower rate if diffusive communication is the rate-limiting step (note, for calculating the first-passage-times, we took the mean end distance for asymmetric ends). However, in contrast to these expectation, we found that, within error, there was no difference between the cleavage rates (Fig. S8*a*). Moreover, within the time resolution limits of these assays (≈1 s), there is no clear lag dependence that could be explained by either directional translocation or bidirectional sliding. Given that diffusive communication is likely to be much faster than the overall cleavage rate on these length scales (see above), it is perhaps unsurprising that we were unable to observe a clear distance-dependent relationship using this approach.

The data in Fig. S8*a* suggests that the actual diffusion process can be considered as instantaneous compared with the total cleavage time. We therefore tried to design a new set of measurements by limiting the number of enzyme collisions as function of DNA length. One way to stimulate cleavage of linear DNA is to cap the DNA ends as, within our model, any diffusing enzyme should not fall off the DNA and with sufficient diffusion time be able to find its target. On uncapped DNA, however, a diffusing enzyme will either reach the end and either fall off or find its target site. The probability P_{target} that an enzyme will find its target site at a distance d and not fall off before at the DNA end at distance e is given by (11):

$$P_{target} = \frac{e}{d + e}$$

Thus, if the number of enzyme collisions limits cleavage, the cleavage rate should scale with the DNA end length according to this relationship. We note that Eq. **3** provides only the scaling of the rates and not their magnitude. The latter would be determined by the actual enzyme turnover, that is, mainly by the relative values of k_{on} and k_{off}. The scaling relationship of Eq. **3** is only expected if, on the time scale of the diffusion process (τ), the target is always occupied by an enzyme, that is, $1/k_{ini} \gg \tau$. To test such a potential scaling behavior, we constructed four symmetric DNA substrates with a constant 100-bp intersite spacing and varying, symmetrical DNA end lengths of 100 bp, 200 bp, 500 bp, and 1000 bp (Fig. S8*b*). To detect the short DNA substrates, we increased the DNA concentration and moderately adjusted the enzyme concentration. For these conditions and for the substrates used, we had readily detectable cleavage activity for the uncapped substrates, although with lower efficiencies than the equivalent capped DNA. Determining the cleavage rates for the different substrates provided a strong dependency on the length of the DNA ends (Fig. S8*b*) in contrast to the capped DNA substrates, which, within error, did not exhibit such a dependency (data not shown). This is in strong support of our hypothesis expounded above. However, fitting *SI Text* Eq. **3** to the data did not provide a good quantitative agreement as the measured rates changed much more severely than predicted. This is not really surprising because the equation holds only if the target site is always occupied by an enzyme, that is, for a narrow window of possible parameters. However, by allowing the target enzyme to dissociate and associate with certain rates, the dependency of P_{target} on the DNA end length can provide a reasonable agreement with the measured data (Fig. S8*b*), although we note that the chosen parameters are somewhat arbitrary and other parameter configurations can also provide a similar dependency.

Nonetheless, despite the lack of strong quantitative agreement with Eq. **3**, the dependency of the cleavage rate on the DNA end length for uncapped DNA provides solid support for a random bidirectional stepping, that is, the diffusion model of Fig. S6. Directional translocation models cannot explain the observed *increase* of the cleavage rate with *increasing* end length. For a

undirectional translocation scheme, one would expect there to be no dependency on the end length. For a bidirectional scheme, in which enzymes translocate 50% of time leftward and 50% of the time rightward, those enzymes that moved toward an end would spend longer going in the "wrong" direction and therefore one would expect the cleavage rate to decrease with increasing distance, the complete opposite of our observations. One might still argue that a translocating enzyme could by chance turn around during translocation with a given rate and therefore provide the observed end length dependency. However, this is then nothing else but a random walk along the DNA and would, if one cannot resolve the individual bp steps of the enzyme, be indistinguishable from diffusion. Even recent single-molecule fluorescence experiments observing the diffusion of individual enzymes would not be conclusive, because the typical time resolution of these measurements represents an average of a great many steps. However, given the low levels of ATP consumed per successful cleavage event, such a translocation-driven random walk appears not very likely at all.

In summary, the end length dependence of cleavage provides additional support for intersite communication based on diffusion. However, a quantitative understanding of the whole cleavage process requires extensive characterizations of the individual steps by using both bulk and single molecule experiments and is outside the scope of the current study.

Methods

Calculating the Time Resolution. At high forces, the time resolution is limited by the acquisition time of the camera (16.7 ms, 60 Hz acquisition frequency). We note, however, that at high forces (i.e., 1.5 pN and 5 pN used here) one can still detect events which are significantly shorter than the acquisition time limit because of the greatly reduced noise. Such fast looping events would be seen as spikes whose amplitude would be shorter than the full looping distance but which would be noticeably greater than the background noise.

At low forces the amplitude of the Brownian motion of the magnetic particle is larger than the looping distance. Therefore, one has to average over a longer time to reliably determine the DNA length and to detect length changes.

The observed dynamics of the Brownian fluctuations of the magnetic sphere-DNA system after averaging the signal over time t_{aver} is given by the following noise power spectrum (15):

$$S_z^{aver}(f) = \frac{4k_BT\gamma_{trans}}{k_{DNA}^2} \quad \frac{1}{1+(f/f_c)^2} \quad \frac{\sin^2(\pi f \cdot t_{aver})}{(\pi f \cdot t_{aver})^2}$$

Here, k_B denotes the Boltzmann constant and T the temperature. The so-called cut-off frequency, f_c, obeys the relation $f_c = k_{DNA}/2\pi\gamma_{trans}$. γ_{trans} is the drag coefficient of the magnetic sphere given by the Stokes relation and k_{DNA} is the longitudinal stiffness of the DNA, which in the limits of small displacements is obtained by derivation of the DNA force-extension relation (16). Integration of $S_z^{aver}(f)$ now provides the residual mean-square fluctuation $\langle z^2\rangle^{aver}$ of the magnetic sphere after averaging. To reliable detect a step of length L_{step}, L_{step} has to be four times larger than $\sqrt{\langle z^2\rangle^{aver}}$ (This corresponds to a signal-to-noise ratio of 4, which is typically considered to be sufficient for reliable step detection). Therefore, the time resolution determined by the averaging time t_{aver}, for which $\sqrt{\langle z^2\rangle^{aver}}$ becomes 4 times smaller than L_{step}. We computed the time resolution as function of force (Fig. S1) numerically by iteratively finding the t_{aver}, which fulfils the condition. For L_{step}, the contour length of the DNA in the loop corrected by the relative extension of the DNA at the given force was used.

Calculating the Minimum Looping Time at High Forces. At the higher applied forces of 1.5 and 5 pN, the time resolution is set by the camera and theoretically we are not able to detect events shorter than 1 ms in duration. However, at these forces the DNA extension of the full molecule is larger than the remaining contour length after looping. This means that loop formation is not primarily limited by the intrinsic DNA energetics and hydrodynamics, but simply by the position and dynamics of the magnetic sphere, which has to be at least at a distance shorter than the contour length after looping. Thus, by calculating the mean time taken for the bead to eventually diffuse to this position under the influence of the external forces, we can obtain the minimum average loop-formation time. Because of the force dependency of loop formation itself, the actual loop formation time is, in fact, much higher. However, the theoretical dynamics of DNA loop formation as function of tension has not been worked out at present.

The motion of the magnetic sphere can be described as diffusion within a harmonic potential with spring constant k_{DNA} (see above). The mean-time to diffuse a distance L_{loop} of the equilibrium position is then given by (12):

$$T_{loop} = \frac{\gamma_{trans}}{k_{DNA}} \quad \sqrt{\frac{\pi}{4}} \quad \sqrt{\frac{2k_BT}{k_{DNA}L_{loop}^2}} \exp\left(\frac{k_{DNA}L_{loop}^2}{2k_BT}\right)$$

As can be seen (Fig. S1), by using our constructs and the applied forces (1.5 and 5 pN), it would take, at a minimum, several thousand years before the magnetic bead would reach a position which would allow loop formation. Consequently, the probability that any of our observed cleavage events were preceded by DNA looping is vanishingly small.

1. Gorman J, *et al.* (2007) Dynamic basis for one-dimensional DNA scanning by the mismatch repair complex Msh2-Msh6. *Mol Cell* 28:359–370.
2. Helenius J, Brouhard G, Kalaidzidis Y, Diez S, Howard J (2006) The depolymerizing kinesin MCAK uses lattice diffusion to rapidly target microtubule ends. *Nature* 441:115–119.
3. Janscak P, Sandmeier U, Szczelkun MD, Bickle TA (2001) Subunit assembly and mode of DNA cleavage of the type III restriction endonucleases EcoP1I and EcoP15I. *J Mol Biol* 306:417–431.
4. Meisel A, Mackeldanz P, Bickle TA, Krüger DH, Schroeder C (1995) Type III restriction endonucleases translocate DNA in a reaction driven by recognition site-specific ATP hydrolysis. *EMBO J* 14:2958–2966.
5. Mücke M, Reich S, Möncke-Buchner E, Reuter M, Krüger DH (2001) DNA cleavage by type III restriction-modification enzyme EcoP15I is independent of spacer distance between two head to head oriented recognition sites. *J Mol Biol* 312:687–698.
6. Blainey PC, van Oijen AM, Banerjee A, Verdine GL, Xie XS (2006) A base-excision DNA-repair protein finds intrahelical lesion bases by fast sliding in contact with DNA. *Proc Natl Acad Sci USA* 103:5752–5757.
7. Granéli A, Yeykal CC, Robertson RB, Greene EC (2006) Long-distance lateral diffusion of human Rad51 on double-stranded DNA. *Proc Natl Acad Sci USA* 103:1221–1226.
8. Tafvizi A, *et al.* (2008) Tumor suppressor p53 slides on DNA with low friction and high stability. *Biophys J* 95:L01–L03.
9. Komazin-Meredith G, Mirchev R, Golan DE, van Oijen AM, Coen DM (2008) Hopping of a processivity factor on DNA revealed by single-molecule assays of diffusion. *Proc Natl Acad Sci USA* 105:10721–10726.
10. Bonnet I, *et al.* (2008) Sliding and jumping of single EcoRV restriction enzymes on non-cognate DNA. *Nucleic Acids Res* 36:4118–4127.
11. Berg HC (1993) *Random walks in biology* (Princeton Univ Press, Princeton, NJ).
12. Howard J (2001) *Mechanics of Motor Proteins and the Cytoskeleton* (Sinauer Associates, Sunderland, MA).
13. Szczelkun MD (2002) Kinetic models of translocation, head-on collision, and DNA cleavage by type I restriction endonucleases. *Biochemistry* 41:2067–2074.
14. McClelland SE, Dryden DTF, Szczelkun MD (2005) Continuous assays for DNA translocation using fluorescent triplex dissociation: Application to type I restriction endonucleases. *J Mol Biol* 348:895–915.
15. Gittes F, Schmidt CF (1998) *Methods in cell biology.*, vol. 55 (Academic).
16. Bouchiat C, *et al.* (1999) Estimating the persistence length of a worm-like chain molecule from force-extension measurements. *Biophys J* 76:409–413.
17. Firman K, Szczelkun MD (2000) Measuring motion on DNA by the type I restriction endonuclease EcoR124I using triplex displacement. *EMBO J* 19:2094–2102.
18. Saha A, Wittmeyer J, Cairns BR (2002) Chromatin remodeling by RSC involves ATP-dependent DNA translocation. *Genes Dev* 16:2120–2134.
19. Sivanathan V, *et al.* (2006) The FtsK gamma domain directs oriented DNA translocation by interacting with KOPS. *Nat Struct Mol Biol* 13:965–972.

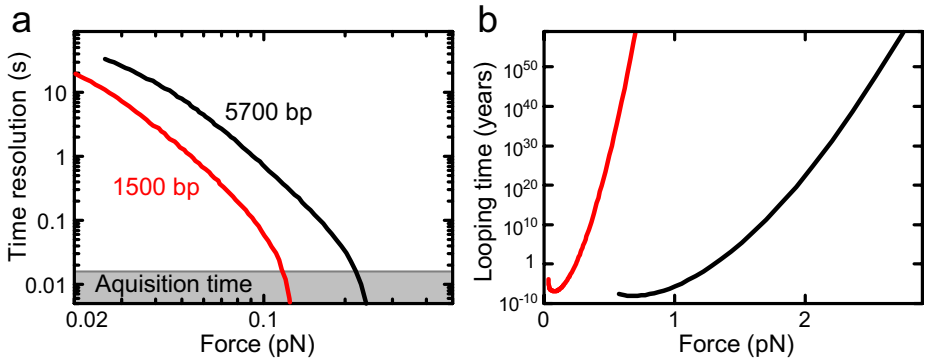

Fig. S1. Time resolution of the magnetic tweezers measurements and minimum high force looping time. (*a*) Time resolution to detect a 1,100-bp loop on a DNA molecule with 1,500 bp (red) and 5,700 bp (black) length as a function of force calculated as described above in *SI Text*. At low forces the amplitude of the Brownian motion of the end of the DNA molecule are larger than the DNA loop length. Therefore, one has to average over a certain time to reliably detect a loop of a given size (see 0.1 pN trace in Fig. 3*A*). The time resolution calculated here is the minimum averaging time to achieve a signal-to-noise ratio of four, which is generally considered to allow a reliable step determination. At high force the time resolution becomes limited by the acquisition time of the camera recording images at 60 Hz (i.e., 16.7 ms). Nonetheless at high enough forces such as 1.5 pN and 5 pN, transient loops with significantly shorter life times (down to 1 ms) would still be detectable as transient spikes with an amplitude shorter than 1,100 bp but significantly above the detected bead noise. The calculations have not been extended to include this since at these forces transient diffusive loops of 1,100-bp size will not form at all at experimentally relevant time scales (see part *b*). Note that the time resolution in the tethered particle experiments (at ≈0.01 pN) is significantly better (≈1 s) because of the detection of the lateral RMS amplitude as can be seen in the experiments with *Nae*I (Fig. 4*B*). (*b*) Minimum average looping time for a 1,100-bp loop as function of force for DNA molecules with 1,500 bp (red) and 5,700 bp (black) length. It is the average time one has to wait to see the magnetic bead by chance at a position that corresponds to DNA length minus loop length, assuming complete stretching. This is the minimum bead displacement which would allow a loop to be formed. We note that this time is even larger if one also considers more realistic force-dependent, noncomplete DNA stretching. For any of the constructs used here, loops can be ruled out at forces of 1.5 and 5 pN given the average length of our experiments and the minimum looping time of 10^x years ($x > 4$). At low forces the curves cannot be calculated because the DNA extension is then lower than the DNA contour minus the loop length.

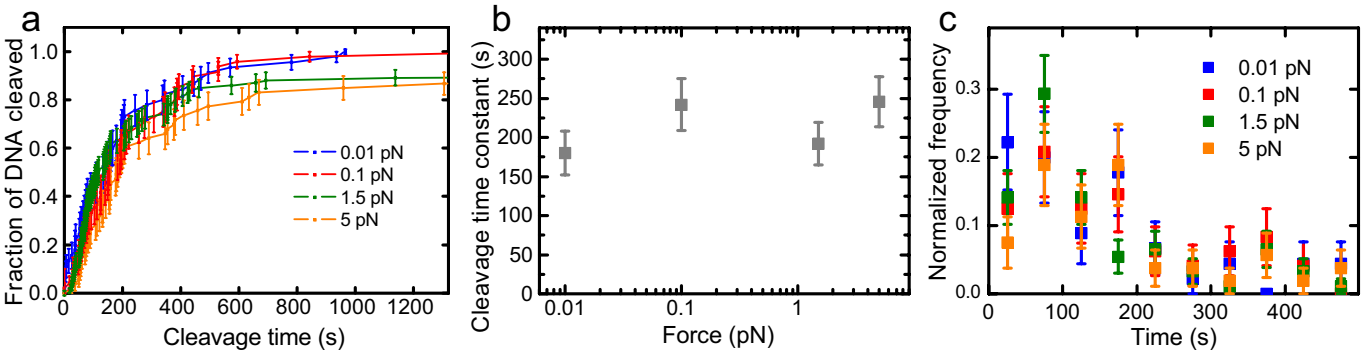

Fig. S2. Force dependency of DNA cleavage by *Eco*PI and associated errors. (*a*) Single molecule cleavage kinetics from Fig. 3*C* with associated statistical errors. Error bars are calculated as the standard deviation of the binomial distribution $[p(p\text{-}1)/N]^{1/2}$, where p is the fraction of molecules cleaved and N is the total number of molecules. Within error all four curves show a significant overlap for times $<$400 s, that is, deviations lie within the statistical error. For times larger than 400 s, small but statistically relevant deviations occur (see below). (*b*) Cleavage time constant from simple exponential fits (amplitude and time constant as parameters) as function of force. Errors represent the error from fitting the data plus a 10-s time uncertainty error from flushing in the enzyme. The cleavage time constant does not, within error, reveal a force dependence. We note however, that for the cleavage amplitude a trend of a slightly reduced cleavage amplitude with increasing force is observed. At the moment we do not understand the origin of the incomplete cleavage. This might be due to a slow autoinhibition of the enzyme or because of background methylation at its site, either of which might be force-dependent. This needs to be determined in more detail in the future. However, for the experiments here the observed rate of initial cleavage is of much more relevance, and, within error, remains constant over almost three orders of magnitude of applied forces. Given the expected strong force dependence for diffusive DNA looping (Fig. 4*A*), the minor effect observed on the cleavage amplitude does not weaken our conclusion on the absence of DNA looping. (*c*) Overlayed histograms from Fig. 3*B* with error bars. The histograms overlap well within the given errors and no significant systematic change can be observed for the given statistical errors.

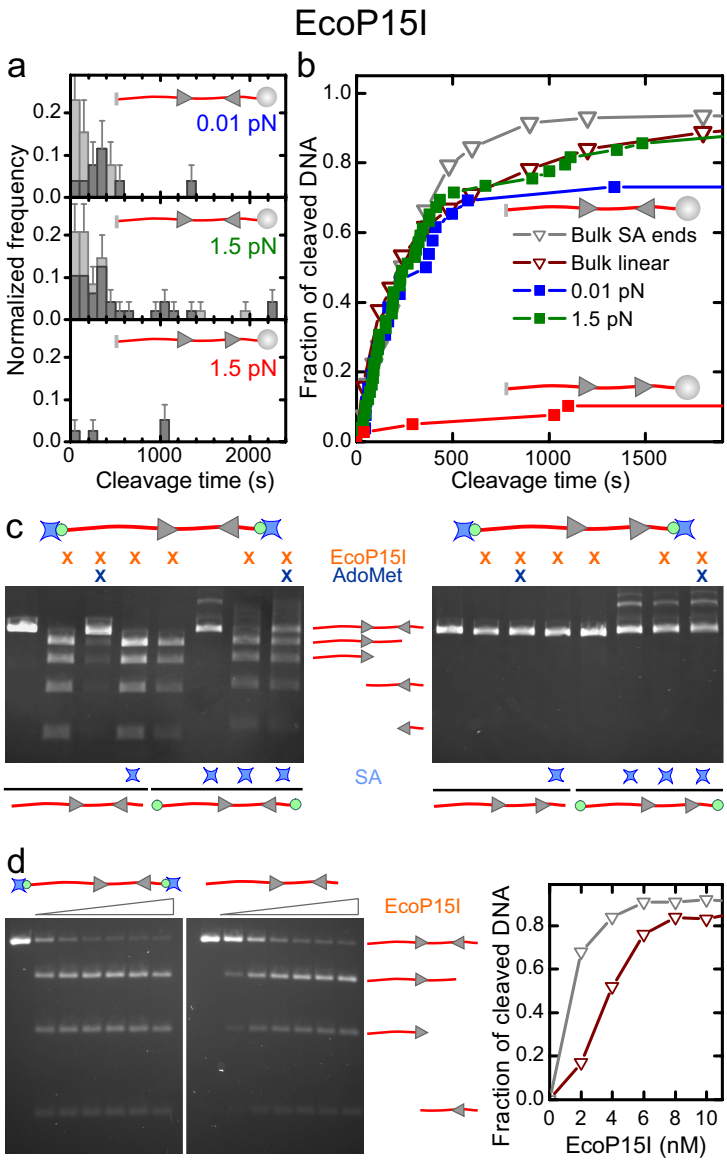

Fig. S3. Single-molecule and bulk DNA cleavage by *Eco*P15I. (*a*) Histograms of the cleavage times for a HtH substrate at 0.01 pN ($n = 26$) and 1.5 pN ($n = 48$) and a HtT substrate at 1.5 pN ($n = 39$). For both substrates the intersite distance is 1.0 kb. As for *Eco*PI, cleavage is orientation-specific with slow and inefficient cleavage (≈10%) for the HtT substrate and, fast and efficient cleavage (≈90%) for the HtH substrate. No significant difference in the cleavage time distribution between 0.01 pN (random coil) and 1.5 pN (89% stretched) was observed. At 1.5 pN, cleavage was never preceded or accompanied by DNA loop formation between the two *Eco*P15I sites ($n = 48$). Cleavage time distributions for intact (unnicked) molecules (gray bars) are very similar compared with all molecules (light gray bars). (*b*) Cleavage kinetics from the tweezers compared with those obtained in bulk experiments with and without streptavidin (SA) capped ends. For both substrates, cleavage profiles were obtained that were nearly identical (cleavage of the uncapped DNA being slightly less efficient) and that were similar to the profiles obtained in the single-molecule measurements. This lends additional support to the idea that DNA looping is not needed for efficient intersite communication. (*c*) Effect of DNA-end capping by streptavidin on the cleavage efficiency in bulk experiments. Conditions and indices are as in Fig. 3*D* (main text) except that *Eco*P15I was taken. The results are slightly different from the findings for *Eco*PI, where we found a more significant effect on end capping. Nonetheless, *Eco*P15I is greatly stimulated by end-capping in the presence of AdoMet. In general, *Eco*P15I is more efficient in cleaving uncapped linear DNA than *Eco*PI. However, we note that at reduced *Eco*P15I concentrations a stimulation from end-capping is also observed without AdoMet (see part *d*). *Eco*P15I substrates were made analogously to *Eco*PI substrates, by using pMDS60a (4,374 bp, HtH oriented sites with 952-bp spacing) and pMDS60b (4,375 bp, HtT oriented sites with 931-bp spacing). After digestion with *Xba*I and/or *Not*I the *Eco*P15I sites were located approximately 0.8 kb and 2.6 kb from the ends. (*d*) Cleavage efficiency of *Eco*P15I on capped (gel picture on the *left*) and uncapped DNA (gel picture on the *right*) as function of the *Eco*P15I concentration. Conditions were as in *C*, that is, 2 nM DNA, except that the *Eco*P15I concentration was changed. *Eco*P15I concentrations from left to right lanes were 0, 2, 4, 6, 8, 10, and 15 nM. The plot on the *right* was obtained by quantifying the amount of DNA cleaved. Gray and brown triangles are for capped and uncapped DNA, respectively. As can be seen, cleavage is much more efficient on capped DNA at lower enzyme concentration, providing evidence for the stimulatory effect of capped DNA ends also for EcoP15I in the absence of AdoMet. Given the simple cleavage model we propose (see Fig. S6 and *SI Text*) one can readily explain the more efficient DNA cleavage by *Eco*P15I on linear DNA. For example, by simply increasing k_{on} relative to k_{off}, the lifetimes of the enzyme during sliding and at the site will increase, leading to more loading of enzymes on the DNA per unit time and more chance of collision and thus cleavage. Only at low enzyme concentrations, where occupancy is limited to a few enzymes per DNA will the end-effects become noticeable. The increased ATPase activity of *Eco*P15I is consistent with an increased efficiency of DNA occupancy and thus cleavage.

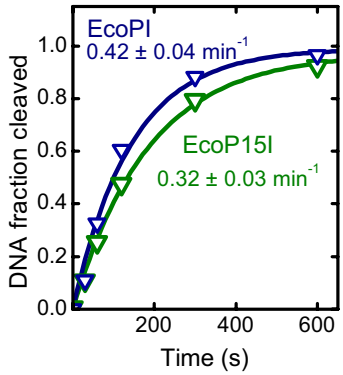

Fig. S4. Bulk cleavage kinetics of capped *Eco*PI and *Eco*P15I substrates taken at 1 mM ATP (scatter data) with corresponding exponential fits (solid lines) and associated cleavage rates. These rates were used to obtain the number of ATPs hydrolyzed per DNA cleavage event.

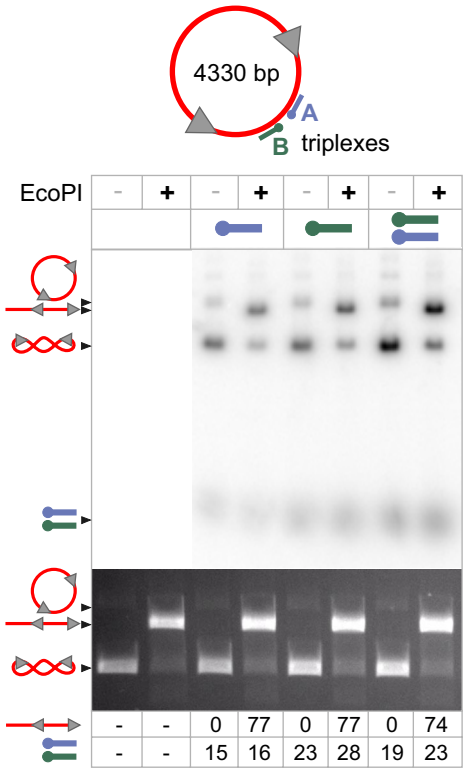

Fig. S5. EcoPI does not displace DNA triplexes. dsDNA translocation in the absence of DNA unwinding can be efficiently measured in a biochemical assay by the displacement of small triplexes bound at specific sites on the DNA (14, 17). This assay has been used to measure motor activity of a number of bona-fide dsDNA translocases, including Type I REs (14, 17), chromatin remodeling enzymes (18), and DNA pumps such as FtsK (19). We therefore tested the activity of *Eco*PI by using plasmids with two HtH sites spaced approximately 1.6 kb apart, between which two separate 22-bp long triplex binding sites with opposite orientations had been introduced. Under the conditions here, the efficiency of circular DNA cleavage is equivalent to capped linear DNA (data not shown). Distinct to dsDNA motors, no triplex displacement was observed independent of the triplex orientation. In addition, the efficiency (see Figure) and rate (data not shown) of DNA cleavage was unaffected by triplex binding suggesting that *Eco*PI can bypass the roadblocks. Because the presence of a flap has been shown to assist motor-driven triplex dissociation in some cases (19), similar experiments were carried out by using triplexes with 3 and 10 nt long 3′ flaps providing the same negative result (unpublished observation). Triplex reactions were carried out as described in ref. 17. Triplex sequences were: A, 5′-TTCTTTTCTTTCTTCTTTCTTT-3′; and B, 5′-TTTCTTCTTCTTTTCTTTTCTT-3′. Plasmid DNA (see above) was bound with a 2-fold excess of either triplex A, B, or both. Cleavage reactions contained 5 nM triplex-bound DNA, 30 nM *Eco*PI, 4 mM ATP, and 100 μM AdoMet in buffer R. Reactions were incubated at 20°C as indicated and stopped by addition of 0.25 volumes of 15% (wt/vol) glucose, 3% (wt/vol) SDS, 250 mM Mops (pH 5.5), and 0.4 mg/ml bromophenol blue. Reaction products were separated by agarose gel electrophoresis. Percentages of DNA cut and triplex bound were calculated by gel densitometry.

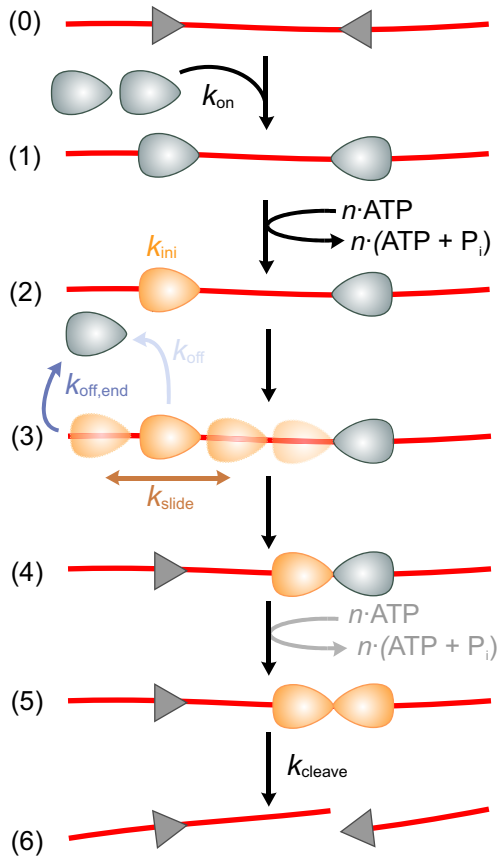

Fig. S6. Detailed model for the intersite communication by Type III REs based on 1D- diffusion. [1] Enzymes (gray ovals) bind to their asymmetric sites in a defined orientation onto DNA each with a concentration dependent rate k_{on}. [2] An enzyme switches into the diffusion mode (orange oval) with rate k_{ini}. We speculate that this is triggered by ATP binding and/or hydrolysis similar to the kinesin-related protein MCAK for which the ATP hydrolysis state determines whether it diffuses or not (2). [3] Enzyme(s) diffuse along DNA in a 1D fashion with k_{slide} in a bidirectional random walk. During sliding the enzyme can reach the DNA end and dissociate on uncapped DNA with $k_{off,end}$. We anticipate that simple dissociation (k_{off}) during sliding occurs less frequent, because DNA end-capping can have tremendous influence over distances of several kb. [4] 1D diffusion is stopped on collision with a second enzyme, which can still be bound on a second target site. [5] If the enzymes are in a correct orientation, that is, HtH, both enzymes can cooperate in a process, which probably relies on ATP hydrolysis (3) and [6] trigger DNA cleavage with k_{cleave}.

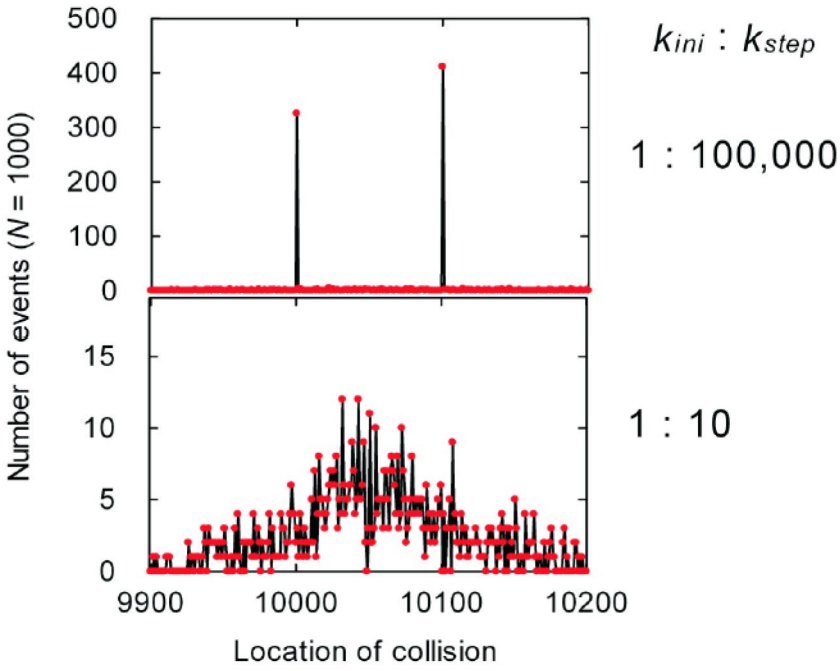

Fig. S7. Collision location obtained from simulations for different ratios of k_{ini}:k_{step}. Sliding was simulated by Monte Carlo methods as follows. Two enzymes were modeled as prebound to a DNA lattice of >20,000 bp, with the molecules located initially at positions 10,000 and 10,100 (i.e., 100 bp apart). The long lattice was chosen to avoid the problem of DNA ends. Initiation of sliding occurred with a rate constant k_{ini}. After initiation, movement leftward or rightward on the DNA occurred with a rate constant k_{step}. When both enzymes occupied adjacent locations, a collision event was scored. The simulation was repeated for 1,000 molecules. For pairs which had taken >50 million combined steps without collision, the reaction was rejected as having failed because of dissociation. The data shows that where k_{ini} and k_{step} are similar in value, the majority of collisions occur at random locations on the lattice, with a distribution centered midway between the sites. As sliding becomes faster and initiation slower however, the majority of collisions occur between one sliding and one static enzyme. It should be noted that this distribution will revert to a random one as the intersite distance is increased. However, we suggest that only those cleavages that occur between a diffusing enzyme and a site-bound one produce an active nuclease. Therefore, a drop in cleavage efficiency with very long distance can be explained by either a limiting off rate from the DNA or by the majority of enzyme collisions occurring off-site. Based on the slow ATPase rates we observe and the expectation of comparably fast rates of sliding, the Type III cleavage pattern of 50% at one site and 50% at the other site can therefore be readily explained.

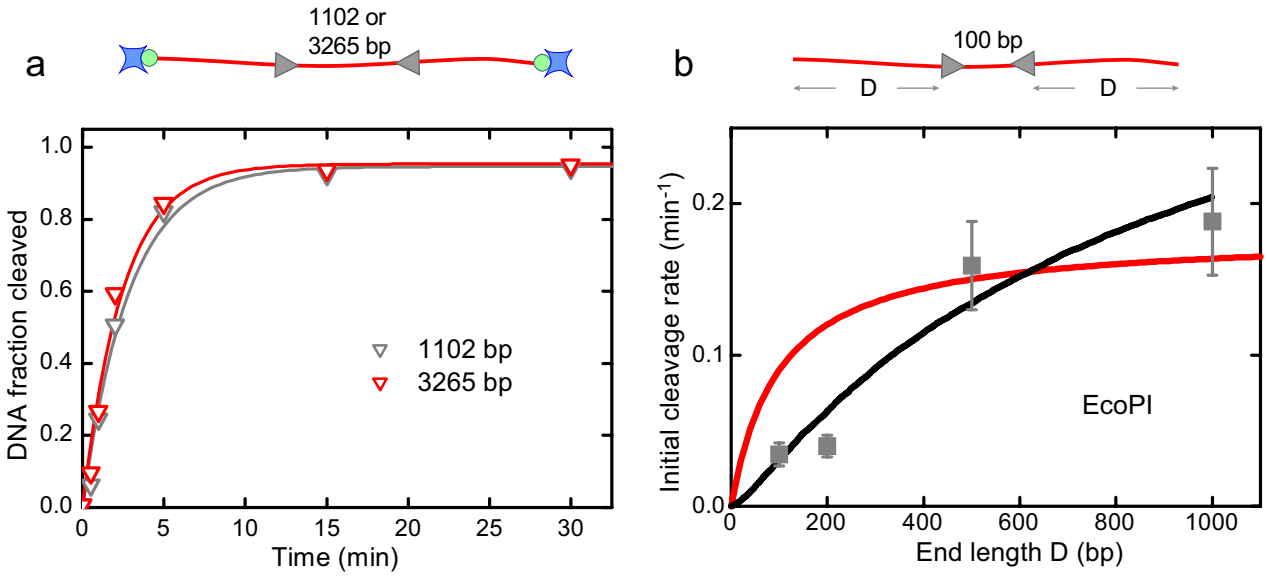

Fig. S8. Cleavage kinetics for DNA substrates with different intersite spacing and different DNA end lengths using *Eco*PI. (*a*) Cleavage kinetics with a streptavidin-capped DNA on a substrate with 1.1-kb intersite distance and end distances of 1.4 and 3.2 kb and on a substrate with 3.3-kb intersite distance and end distances of 1.1 and 1.4 kb. Cleavage rates from simple exponential fits provide 0.35 ± 0.05 min^{-1} and 0.41 ± 0.05 min^{-1} for the substrate with 1.1-kb and 3.3-kb intersite distances, respectively. Within error these rates are equal. Reaction conditions were as described in Materials and Methods, that is, 2 nM DNA, 15 nM *Eco*PI, and 4 mM ATP. (*b*) Initial cleavage rate on uncapped DNA as function of the DNA end length (gray squares). The DNA constructs used were symmetrical, with 100 bp between the two HtH sites and DNA ends with equal lengths of 100, 200, 500, and 1,000 bp length. Reaction conditions were as described in Materials and Methods, except that 10 nM DNA and 20 nM *Eco*PI were used. The DNA concentration was increased to allow detection of the short DNA substrates on the agarose gels. The solid lines are the probability functions for the given DNA lengths that a diffusing enzyme collides with an enzyme at the second target site before falling off the DNA end. This has been calculated assuming that the second enzyme is always present at the site (red line, *SI Text* Eq. **1**) or that the second enzyme associates with k_{on} and dissociates with k_{off} at the target site (black line, $k_{on} = k_{step}/50000$ and $k_{off} = k_{step}/2000$). The black curve was obtained from Monte Carlo simulations. The diffusion of the first enzyme was modeled as a pure random walk (11) with one single bp step with random direction per simulation cycle. Association and dissociation were allowed to occur randomly with a probability of 1/50,000 and 1/20,000, respectively. The simulation was stopped if either the first enzyme has reached the end or if it had reached the second enzyme position, with the second enzyme being associated at the site. Such a simulation was repeated 10,000 times and the number of simulations in which the enzyme collided with the second enzyme divided by the total number of simulations provided the desired probability. Both probability curves have been multiplied by a scaling factor to fit the observed rate measurements. The probability of not falling-off before collision at 1,000-bp end length is 0.91 for the red curve and 0.49 for the black curve. A similar set of experiments with similar substrates and identical conditions was also carried out for *Eco*P15I. For this enzyme we obtained very similar observations, that is, end length-independent cleavage rates on capped substrates and increasing cleavage rates for increasing end lengths (data not shown). In the latter case, the ratio between the rates for longest and shortest ends is approximately four as observed for *Eco*PI.